



## Amorphous oxygencontaining hydrogenated carbon films formed by plasma enhanced chemical vapor deposition

Steven F. Durrant, Sandra G. Castro, Jorge I. Cisneros, Nilson C. da Cruz, and Mário A. Bica de Moraes

Citation: *Journal of Vacuum Science & Technology A* **14**, 118 (1996); doi: 10.1116/1.579906

View online: <http://dx.doi.org/10.1116/1.579906>

View Table of Contents: <http://scitation.aip.org/content/avs/journal/jvsta/14/1?ver=pdfcov>

Published by the AVS: Science & Technology of Materials, Interfaces, and Processing

### Articles you may be interested in

Preparation of hydrogenated amorphous germanium nitrogen alloys by plasma enhanced chemical vapor deposition

J. Appl. Phys. **80**, 4703 (1996); 10.1063/1.363454

Deposition of hydrogenfree diamondlike carbon film by plasma enhanced chemical vapor deposition

Appl. Phys. Lett. **68**, 3594 (1996); 10.1063/1.116648

Nitrogen doped fluorinated amorphous carbon thin films grown by plasma enhanced chemical vapor deposition for low dielectric constant interlayer dielectrics

Appl. Phys. Lett. **68**, 3656 (1996); 10.1063/1.115761

Fluorinated amorphous carbon thin films grown by helicon plasma enhanced chemical vapor deposition for low dielectric constant interlayer dielectrics


Appl. Phys. Lett. **68**, 2864 (1996); 10.1063/1.116350

Formation of electrically conductive nitrogendoped amorphous hydrogenated carbon (diamondlike carbon) films by the supermagetron plasma chemical vapor deposition method

J. Vac. Sci. Technol. A **14**, 1933 (1996); 10.1116/1.580363



## Instruments for Advanced Science


Contact Hiden Analytical for further details:  
 [www.HidenAnalytical.com](http://www.HidenAnalytical.com)  
 [info@hiden.co.uk](mailto:info@hiden.co.uk)

[CLICK TO VIEW](#) our product catalogue



**Gas Analysis**

- › dynamic measurement of reaction gas streams
- › catalysis and thermal analysis
- › molecular beam studies
- › dissolved species probes
- › fermentation, environmental and ecological studies



**Surface Science**

- › UHV TPD
- › SIMS
- › end point detection in ion beam etch
- › elemental imaging - surface mapping



**Plasma Diagnostics**

- › plasma source characterization
- › etch and deposition process reaction
- › kinetic studies
- › analysis of neutral and radical species



**Vacuum Analysis**

- › partial pressure measurement and control of process gases
- › reactive sputter process control
- › vacuum diagnostics
- › vacuum coating process monitoring

# Amorphous oxygen-containing hydrogenated carbon films formed by plasma enhanced chemical vapor deposition

Steven F. Durrant

*Laboratório de Processos de Plasma, Instituto de Física Gleb Wataghin, Universidade Estadual de Campinas, 13083-970, Campinas, São Paulo, Brazil*

Sandra G. Castro

*Grupo de Física de Superfícies, Instituto de Física Gleb Wataghin, Universidade Estadual de Campinas, 13083-970, Campinas, São Paulo, Brazil*

Jorge I. Cisneros

*Grupo de Conversão Fotovoltaica, Instituto de Física Gleb Wataghin, Universidade Estadual de Campinas, 13083-970, Campinas, São Paulo, Brazil*

Nilson C. da Cruz and Mário A. Bica de Moraes

*Laboratório de Processos de Plasma, Instituto de Física Gleb Wataghin, Universidade Estadual de Campinas, 13083-970, Campinas, São Paulo, Brazil*

(Received 13 July 1995; accepted 30 September 1995)

Films were deposited from glow discharge plasmas of acetylene–oxygen–argon mixtures in a deposition system fed with radio frequency power. The principal variable was the proportion of oxygen in the gas feed,  $X_{\text{ox}}$ . The chemical structure and elemental composition of the films were investigated by transmission infrared spectrophotometry and x-ray photoelectron spectroscopy. Optical properties—refractive index, absorption coefficient, and optical gap—were determined from transmission ultraviolet-visible spectroscopy data. The latter also allowed the determination of film thicknesses and hence deposition rates. It was found that the oxygen content of the films and, within limits, the refractive index are controllable by the selection of  $X_{\text{ox}}$ . © 1996 American Vacuum Society.

## I. INTRODUCTION

It has been known for thirty years that amorphous hydrogenated carbon films can be readily deposited from glow discharges of hydrocarbons.<sup>1</sup> The structure of the deposited material depends strongly on the deposition parameters such as the gas pressure, the power applied to the discharge, and the substrate bias voltage and temperature. From a suitable choice of these, a soft, highly cross-linked polymer<sup>2</sup> or a hard, diamondlike material<sup>3</sup> may be produced. Addition of inorganic substances to the hydrocarbon discharge may also cause important changes in film structure and composition. Successful examples of this procedure are the incorporation of nitrogen and fluorine into materials deposited from discharges in which the hydrocarbon component is mixed with nitrogen<sup>4–6</sup> or with fluorine-containing<sup>7–9</sup> compounds. Oxygen may be also incorporated into the film material if an oxygen-containing organic compound is used as a monomer, i.e., the starting material, as in the case of organosiloxanes,<sup>10</sup> or if oxygen-containing substances, such as CO and H<sub>2</sub>O, are used as a comonomer.<sup>11</sup> Oxygen atoms cause polymer etching in glow discharges<sup>12</sup> but the presence of hydroxyl and carbonyl groups in films deposited from hydrocarbon–O<sub>2</sub> discharges shows that oxygen is also chemically incorporated into the film structure.<sup>13</sup>

As reported in another investigation,<sup>14</sup> oxygen produces significant plasma concentrations of the species CO and OH in C<sub>2</sub>H<sub>2</sub>–O<sub>2</sub>–Ar discharges and also contributes to the formation of species that do not themselves contain oxygen, such as CH. Since CH and OH (both free radicals) are very

likely precursors of film formation, the increase in both CH and OH plasma concentrations due to oxygen gives clues as to how oxygen contributes to film formation.

In this work we report on the structural and optical properties of polymer films deposited from C<sub>2</sub>H<sub>2</sub>–O<sub>2</sub>–Ar plasmas at various proportions of oxygen in the feed. Structural features were delineated by transmission infrared (IR) spectroscopy and x-ray photoelectron spectroscopy (XPS). Transmission ultraviolet-visible spectroscopy (UVS) allowed the determination of film thicknesses and the following optical properties of the films: refractive index, absorption coefficient, and optical gap.

## II. EXPERIMENTAL DETAILS

A full description of the deposition system (in-house design) was recently published.<sup>6</sup> Briefly, it consists of a cylindrical stainless steel chamber, fitted with water-cooled parallel plate electrodes connected to a radio frequency (rf) generator (40 MHz, 100 W maximum power) via an in-line wattmeter and an impedance matching network. The substrates were placed on the grounded electrode (anode).

Prior to deposition, the chamber was pumped by a two-stage rotary pump to about 10<sup>-2</sup> Torr, and subsequently by a diffusion pump to about 10<sup>-5</sup> Torr for several minutes. During the depositions the chamber was continuously evacuated by the rotary pump.

The gases C<sub>2</sub>H<sub>2</sub>, O<sub>2</sub>, and Ar, of minimum purity 99.5%, were fed to the chamber via precision electronic mass flow controllers. Films were deposited at various proportions of

O<sub>2</sub> in the gas feed at a constant rf power of 70 W. The total gas flow and the Ar flow, 8.0 and 2.0 sccm, respectively, were also kept constant. Consequently, both the C<sub>2</sub>H<sub>2</sub> and the O<sub>2</sub> flows varied from one deposition to another.

Crystals of KBr were used as substrates for film infrared analysis using an IR spectrophotometer (Perkin-Elmer, 16PC). For analysis by an ultraviolet-visible spectrophotometer (Perkin-Elmer, Lambda 9), films were deposited onto fused quartz substrates. Both spectrophotometers were operated in the transmission mode.

X-ray photoelectron spectroscopy analysis of films deposited on aluminum substrates was carried out using a McPherson ESCA 36 spectrometer employing the Al *K*α x-ray line (1487 eV) for photoelectron excitation. The atomic ratios were computed from the integrated peak areas of the spectra, corrected for electron escape depth, spectrometer transmittance, and photoelectron cross sections for the photon energy of 1487 eV.<sup>15</sup> To investigate various binding states of the carbon atoms in the film, the carbon 1s spectra were decomposed into various Gaussian peaks using a least-squares fit computer program developed by the Surface Science Group of the State University of Campinas.

The optical parameters were determined using the relationship<sup>16,17</sup>

$$T = \frac{A \exp(\alpha t)}{B \exp(2\alpha t) + C \exp(\alpha t) + D}, \quad (1)$$

which holds for the transmission *T* of light at normal incidence on a system formed by a thin film deposited onto a thick substrate. The parameters  $\alpha$  and *t* are the absorption coefficient and the film thickness, respectively; *A*, *B*, *C*, and *D* are functions of the optical parameters of the film and the substrate. Coherent multiple reflections at the thin film interfaces and incoherent multiple reflections at the thick substrate interfaces are considered in its derivation. The film material should be homogeneous and all interfaces should be plane and parallel. No other restrictions apply to Eq. (1).

In the nonabsorbing region, *T* is fully modulated by the interference of the multiple reflected light in the film and the substrate. Each transmission extrema (maximum or minimum) is found at a wavelength  $\lambda_m$  given by

$$\frac{4nt}{\lambda_m} = m, \quad (2)$$

where *n* is the refractive index and *m* is an integer that can be easily determined.<sup>18</sup>

Using Eq. (2) and  $\alpha=0$  in Eq. (1), we have, when *n* is larger than the refractive index of the substrate, *n<sub>s</sub>*, the transmission at the minima:

$$T_{\min} = \frac{4n_s n^2}{(n_s^2 + n^2)(1 + n^2)}. \quad (3)$$

Equations (2) and (3) allow the determination of *n* and *t*, respectively.

To calculate  $\alpha$ , Eq. (1) is rearranged as follows:

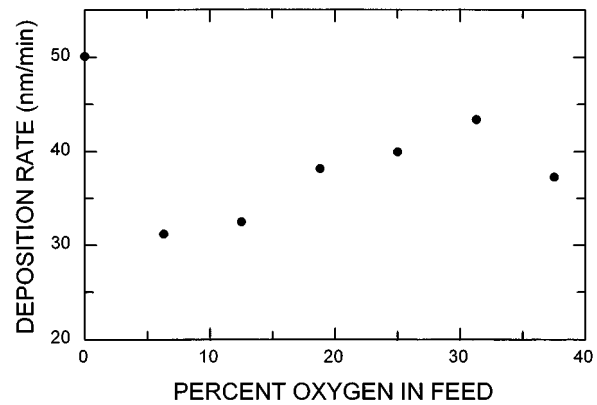


FIG. 1. Deposition rate as a function of the percentage of O<sub>2</sub> in the feed.

$$\exp(\alpha t) = \frac{(A/T - C) + \sqrt{(A/T - B)^2 - 4BD}}{2B}. \quad (4)$$

As *A*, *B*, *C*, and *D* depend weakly on  $\alpha$ , an iterative calculation converges rapidly. This method was used to calculate  $\alpha$  as a function of the photon energy *E*.

### III. RESULTS AND DISCUSSION

#### A. Deposition rate

The film deposition rate *R* is shown in Fig. 1, as a function of the percentage of O<sub>2</sub>, *X<sub>ox</sub>*, in the gas feed. When *X<sub>ox</sub>* varies from 0% to  $\approx 6\%$ , a steep decrease in *R* is produced, from 50 nm/min to a minimum of  $\approx 30$  nm/min. For percentages of O<sub>2</sub> higher than  $\approx 6\%$ , *R* increases at a relatively small rate, reaching a maximum at *X<sub>ox</sub>*  $\approx 30\%$ .

To interpret the dependence of *R* on *X<sub>ox</sub>*, we should first remember that an oxygen plasma is a powerful etchant of organic polymers. The oxygen atoms formed in the discharge react vigorously with the carbon and hydrogen atoms at the polymer surface, forming volatile CO, CO<sub>2</sub>, and H<sub>2</sub>O species<sup>12</sup> which are pumped from the vacuum chamber. On the other hand, in glow discharges containing both oxygen and an organic component, CO, CO<sub>2</sub>, and possibly other species containing C, O, and H arise from gas phase reactions between carbon-containing species and oxygen. In fact, in optical spectroscopy studies of the C<sub>2</sub>H<sub>2</sub>-O<sub>2</sub>-Ar discharges reported earlier,<sup>14</sup> it was shown that the plasma CO concentration increases with increasing proportions of O<sub>2</sub> in the gas feed. As will be shown from IR and XPS analyses in the forthcoming sections, oxygen is incorporated into the deposited material. Thus, oxygen-containing species are among those which, upon adsorption onto the film surface, contribute significantly to film formation. Consequently, film growth in C<sub>2</sub>H<sub>2</sub>-O<sub>2</sub>-Ar discharges must be considered as a balance between the rate of adsorption of the reactive species at the film surface—including oxygen-containing species—and the rate of etching.

According to these ideas, the initial steep decrease in the deposition rate strongly indicates that at small O<sub>2</sub> percentages (up to about 6%), the etching mechanism interferes significantly with film formation. For *X<sub>ox</sub>* values higher than

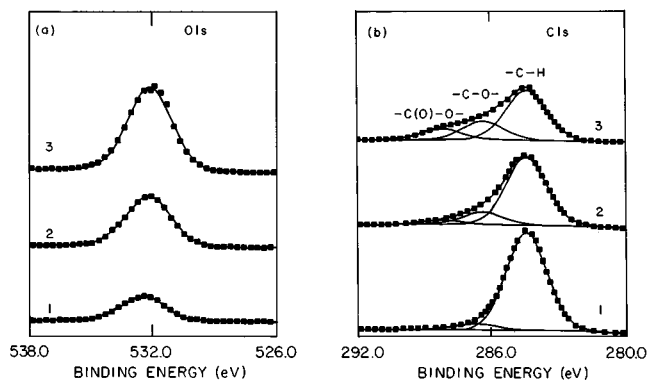


FIG. 2. XPS spectra of films deposited at various percentages of  $O_2$  in the gas feed. (a)  $O 1s$  spectra. (b)  $C 1s$  spectra. Film 1, 0.0%; film 2, 18.8%; film 3, 37.5%.

$\approx 6\%$ , the proportion of atomic oxygen in the discharge—and the etching rate—are expected to increase. However, as  $X_{ox}$  is increased, the plasma concentration of the species contributing to film formation rise faster than the etching rate, and the deposition rate increases.

## B. XPS analysis

Figures 2(a) and 2(b) show, respectively, the  $O 1s$  and  $C 1s$  XPS spectra of three films, labeled 1, 2, and 3, deposited at various values of  $X_{ox}$ . The same x-ray source intensity and the same number of scans were used for all the carbon and the oxygen spectra. As may be seen from Fig. 2(a), the greater incorporation of oxygen into the films as  $X_{ox}$  is increased is indicated by the greater areas of the  $O 1s$  peaks. The ratio  $[O]/[C]$  of the total oxygen to carbon atoms in the films, calculated according to the procedure outlined in Sec. II, is given in Table I. These ratios range from 0.08 to 0.40 as  $X_{ox}$  changes from 0% to 37.5%.

The presence of oxygen in the film obtained without  $O_2$  in the gas feed is attributed to postdeposition reactions. It is known from the literature<sup>19–21</sup> that as-deposited plasma polymers usually contain a large concentration of free radicals. Incorporation of oxygen into the polymer chains thus results from reactions between the free radicals and  $O_2$  and  $H_2O$  molecules from ambient air.<sup>11</sup> In films obtained from  $C_2H_2$  discharges, the free radical concentration is particularly large.<sup>11</sup> As our films were unavoidably exposed to air prior to XPS analysis, the oxygen-containing functionals are formed as a consequence of reactions between these radicals and oxygen and water from the atmosphere. Clearly, these post-deposition reactions are expected to occur also in the films

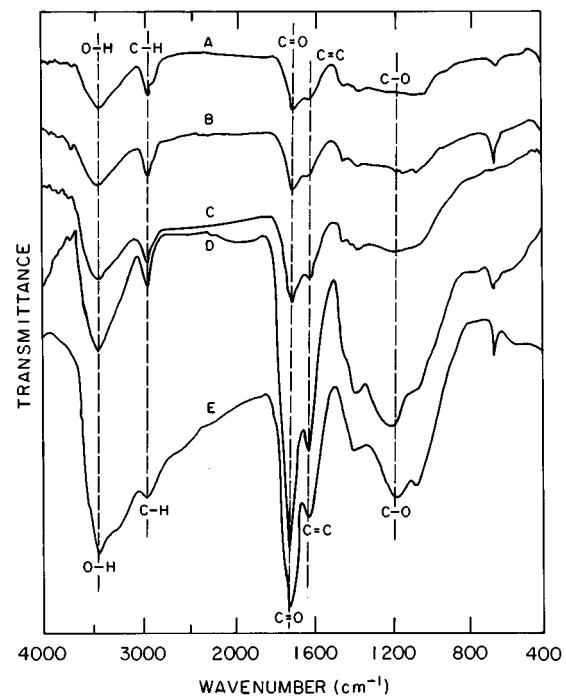


FIG. 3. Transmission IR spectra of films deposited at different percentages of  $O_2$  in the gas feed: (A) 0.0%; (B) 6.3%; (C) 12.5%; (D) 25%; (E) 37.5%. Film thicknesses: (A) 880; (B) 730; (C) 720; (D) 640; (E) 610 nm.

prepared with oxygen in the discharge. In the latter, however, the reaction rates involving  $O_2$  and  $H_2O$  from air should be smaller, as the density of free radicals in polymer films prepared in  $C_2H_2$  discharges containing oxygen is relatively small.<sup>22</sup>

Differences in the  $C 1s$  spectra exhibited in Fig. 2(b) are due to different degrees of incorporation of oxygen into the film structure, which increase from film 1 to film 3. Because of the higher electronegativity of oxygen with respect to carbon, positive binding energy shifts of the  $1s$  electrons of the carbon atoms bound to oxygen are expected. In fact, the  $C 1s$  peak can be resolved into separate gaussian components, the most intense being that due to carbon in hydrocarbon structures at 284.6 eV and the others being at 286.5 and 288.4 eV. As proposed by Clark and co-workers,<sup>23,24</sup> positive  $C 1s$  energy shifts of 1.6 and 4.0 eV are due to ether ( $-C-O-$ ) and carboxyl [ $-C(O)-O-$ ] structures, respectively. Similar energy shifts were obtained here, namely, 1.9 and 3.8 eV, respectively. It is thus clear that the relative rise of the  $C 1s$  peaks at 286.5 and 288.4 eV as  $X_{ox}$  is increased is due to

TABLE I. Ratios of oxygen to carbon atoms and ratios of the carbon atoms in the hydrocarbon  $-C-O-$ , and  $-C-(O)-$  structures, designated  $C_1$ ,  $C_2$ , and  $C_3$  respectively, to the total carbon atoms.

Film	$X_{ox}$ (%)	$[O]/[C]$	$[C_1]/[C]$	$[C_2]/[C]$	$[C_3]/[C]$
1	0.0	0.08	0.930	0.056	0.014
2	18.8	0.20	0.800	0.152	0.048
3	37.5	0.40	0.627	0.236	0.137

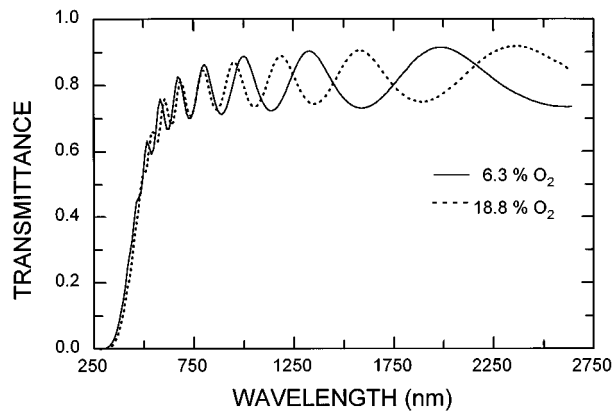


FIG. 4. Ultraviolet-visible transmission spectra of films deposited from an  $C_2H_2-O_2-Ar$  discharge with 6.3% and 18.8%  $O_2$  in the gas feed.

the increase in the concentration of carbon–oxygen bonds in the film material.

Table I also shows the calculated ratios of the carbon atoms in the hydrocarbon,  $-C-O-$ , and  $-C(O)-O-$  structures to total carbon atoms, respectively,  $[C_1]/[C]$ ,  $[C_2]/[C]$ , and  $[C_3]/[C]$ . As we can see from the table, the hydrocarbon structures decrease with increasing  $X_{ox}$  while those associated with oxygen increase. Thus the proportion of oxygen in the deposited material is controllable by selection of  $X_{ox}$ .

### C. Infrared analysis

Figure 3 shows a sequence of IR transmission spectra obtained from films deposited at different values of  $X_{ox}$  in the range 0%–37.5%. The film thicknesses decrease from the film corresponding to spectrum A to that of E.

Consistent with the XPS data, the IR spectra show that oxygen is incorporated into the films. Since the sensitivity of the IR spectrometer was the same for all the spectra of Fig. 3, the increase in the proportion of oxygen in the films as  $X_{ox}$  is increased as evidenced by the increase in the hydroxyl and carbonyl absorption bands peaked at 3450 and 1700  $cm^{-1}$ , respectively. For proportions of  $O_2$  in the feed of 25% and higher, a sudden increase in the oxygen incorporation into the film structure is indicated by the strong increase in these two bands. Also, for these proportions of  $O_2$ , a large density of C–O bonds becomes apparent from the prominent C–O stretching absorption band centered at 1200  $cm^{-1}$ .

The bands peaked at 2950 and 1620  $cm^{-1}$ , corresponding, respectively, to stretching vibrations of the C–H and C=C bonds, are other important features of the spectra. The increase in the C=C stretching absorption amplitudes from spectrum A to E shows that the C=C bond density increases as the proportion of oxygen in the feed is increased. The C–H stretching absorption band, on the other hand, decreases as  $X_{ox}$  is increased, but in spectrum E it is still clearly defined. This observation is again consistent with the XPS results described in Sec. III B. As can be seen from Table I, the ratio  $[C_1]/[C]$  of carbon atoms in hydrocarbon structures to the total carbon atoms decreases from 0.93 to 0.63 as  $X_{ox}$

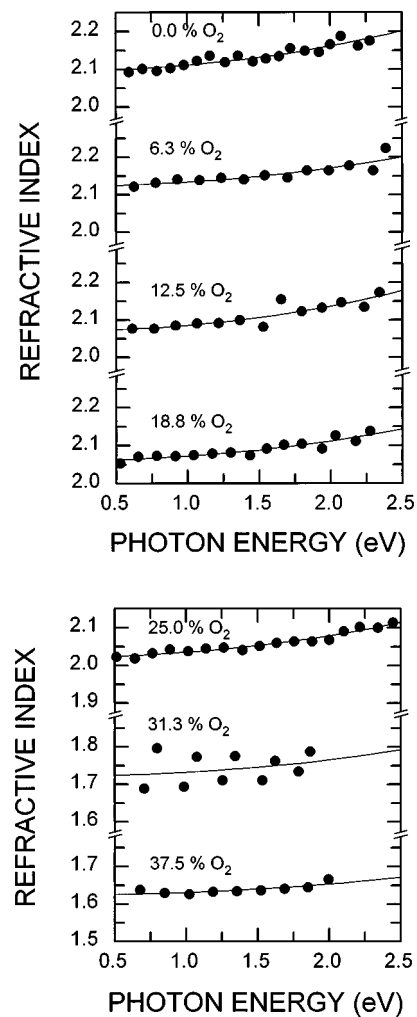


FIG. 5. Experimentally determined refractive index (●) as a function of the photon energy in films deposited at various percentages of  $O_2$  in the gas feed. The continuous lines are least-square fits of the experimental values by the Wemple–DiDomenico equation.

is varied from 0% to 37.5%. Thus, even at high proportions of oxygen in the discharge, a significant density of C–H bonds is still formed in the polymer films.

It should be remembered that the structure of plasma polymers obtained from hydrocarbon–oxygen mixtures generally differ according to the nature of the monomer used and the deposition parameters. As shown by Prohaska and Nickson,<sup>13</sup> the C–H bond density of films prepared from rf discharges of ethylene–oxygen mixtures depends strongly on the proportion of oxygen in the gas feed, and for percentages of  $O_2$  in the gas feed as low as 16%, the C–H stretching absorption is no longer detected in the IR spectrum, indicating that a “pure polycarbonate” film, i.e., a polymer with a negligible hydrocarbon content, is formed. In our study, however, the spectra of Fig. 3 show that polycarbonate-like films of high hydrocarbon and oxygen content can be formed from discharges of  $C_2H_2$ ,  $O_2$ , and Ar mixtures.

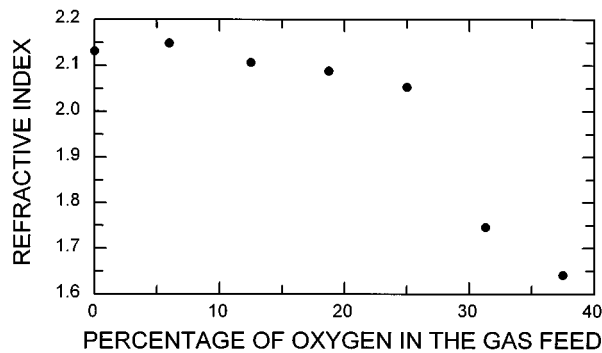


FIG. 6. Refractive index at a photon energy of 1.5 eV as a function of the percentage of O<sub>2</sub> in the gas feed.

#### D. Optical properties

Optical transmission spectra in the range 250–2700 nm of two of the films deposited from the C<sub>2</sub>H<sub>2</sub>–O<sub>2</sub>–Ar discharge onto a quartz substrate are shown in Fig. 4. These spectra are typical of relatively thick (~1 μm) plasma polymer films, showing a very pronounced absorption edge in the ultraviolet region and various interference maxima and minima at higher wavelengths. Also typical of these materials is the high transparency in the near-infrared region. In the spectrum of the film deposited with 6.3% O<sub>2</sub> in the gas feed, for instance, the transmittance at the maxima,  $T_M$ , varies in the infrared region from 0.87 (at 810 nm), to 0.915 (at 1990 nm). The latter  $T_M$  value is very close to the transmittance of the quartz substrate alone (0.92).

The values of the refractive index as a function of the photon energy for various films deposited from the C<sub>2</sub>H<sub>2</sub>–O<sub>2</sub>–Ar discharges are shown in Fig. 5. The continuous line is the least-square fit of the experimental points by the dispersion equation proposed by Wemple and DiDomenico:<sup>25</sup>

$$n^2(E) - 1 = \frac{E_0 E_d}{E_0^2 - E^2}, \quad (5)$$

where  $n$  is the refractive index,  $E$  is the photon energy, and  $E_d$  and  $E_0$  are energy parameters related to the electronic structure of the material. The values of  $E_d$  and  $E_0$  corresponding to the best fit for each film are given in Table II.

The Wemple and DiDomenico (WD) model leading to Eq. (5) is based on one-electron excitation and provides an excellent fit to the experimental dispersion curves  $n(E)$  of a large number of crystalline and amorphous materials. For our films, inspection in Fig. 5 shows that the rise in the refractive index with increasing photon energy can be adequately described by the WD model.

Figure 6 shows the refractive index of the films for the photon energy of 1.5 eV as a function of  $X_{\text{ox}}$ . The values of  $n$  were obtained from the WD curves of Fig. 5. An overall decrease in  $n$  can be seen in the figure as  $X_{\text{ox}}$  is increased. Thus, incorporation of oxygen into the film material decreases the refractive index. The decline in  $n$  is small for proportions of 0%–25% O<sub>2</sub> in the feed but becomes very large in the range 25%–37.5%. We interpret this steep decrease in  $n$  as a consequence of the sudden increase in the

TABLE II. Wemple–DiDomenico parameters for films deposited at various percentages  $X_{\text{ox}}$  of oxygen in the gas feed.

$X_{\text{ox}}$ (%)	$E_0$ (eV)	$E_d$ (eV)
0.0	7.2	24.6
6.3	8.4	29.5
12.5	7.1	23.4
18.8	7.9	25.5
25.0	7.5	23.2
31.3	7.5	14.7
37.5	8.4	13.8

oxygen incorporation into the film material for proportions of O<sub>2</sub> in the gas feed of 25% and higher. The particular value of  $n$  for  $X_{\text{ox}}=31.3\%$  apparently lies considerably off the trend of the curve of Fig. 6. Probably the thickness inhomogeneity of this sample prevented a correct determination of the refractive index. An anomalous behavior of  $n$  vs  $E$  for this film is also observed in Fig. 5.

The optical absorption coefficient  $\alpha$  is plotted in Fig. 7 as a function of the photon energy for various films. In all the films  $\alpha$  rises sharply with  $E$ , as observed for other materials such as amorphous hydrogenated silicon<sup>26</sup> ( $a$ -Si:H) and nitrogenated germanium<sup>27</sup> ( $a$ -Ge:N). As anticipated from Fig. 4, the optical absorption of the films is very low in the low energy region. In the 0–0.5 eV range, the values of  $\alpha$  for some of the films lie below 10<sup>2</sup> cm<sup>-1</sup>. While the dependence of  $\alpha$  on the proportion of oxygen in the gas feed in the photon energy range 0–2.5 eV does not show a well-defined trend, for  $E > 2.5$  eV the absorption coefficient at a given photon energy generally decreases with increasing  $X_{\text{ox}}$ .

The onset of the optical absorption of materials is usually characterized by an optical gap,  $E_g$ . In  $a$ -C:H (Ref. 3),  $a$ -Si:H (Ref. 28), and  $a$ -Ge:N (Ref. 27) films,  $E_g$  is very often determined using Tauc's method,<sup>29</sup> which consists in plotting  $(\alpha n E)^{1/2}$  vs  $E$  and obtaining  $E_g$  from extrapolation of the linear portion of the graph to  $(\alpha n E)^{1/2}=0$ . The  $(\alpha n E)^{1/2}$  vs  $E$  plots for our films, however, do not exhibit a linear region and Tauc's method can not be applied. We have thus defined as an optical gap the photon energy  $E_{04}$  where the absorption coefficient equals 10<sup>4</sup> cm<sup>-1</sup>. This procedure has already been used by Freeman and Paul<sup>28</sup> to characterize amorphous hydrogenated silicon. The gap  $E_{04}$ , determined from the data of Fig. 7, is plotted in Fig. 8(a) as a function of  $X_{\text{ox}}$ . An increase in  $E_{04}$  from 2.62 to 3.21 eV is produced when  $X_{\text{ox}}$  is increased from 0% to 37.5%.

Another point that should be emphasized is the decrease in  $E_{04}$  with increasing refractive index, illustrated in Fig. 8(b) for the values of  $n$  at the photon energies of 0 eV (static refractive index) and 1.5 eV. This behavior is typical of materials such as  $a$ -Si:H and  $a$ -Si:H:N with varying composition and hence varying electronic structure,<sup>30,31</sup> and it can be explained by a relationship between the static refractive index  $n_0$  and the spectrum of the imaginary part of the dielectric function,  $\epsilon_2$ :<sup>32</sup>

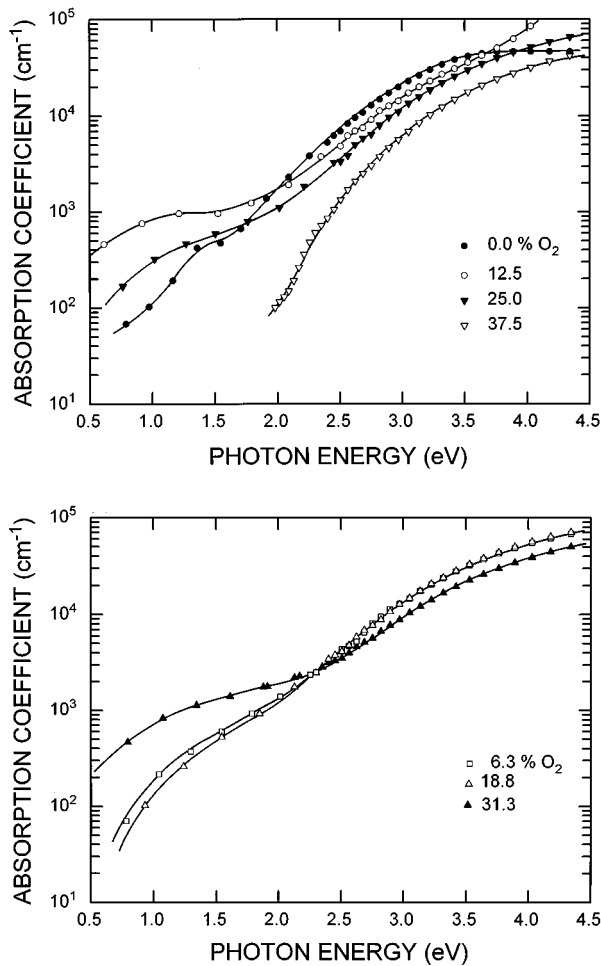


Fig. 7. Dependence of the absorption coefficient on the photon energy for films deposited at several proportions of  $O_2$  in the gas feed.

$$n_0^2 = 1 + \frac{2}{\pi} \int_0^\infty \frac{\epsilon_2(E)}{E} dE. \quad (6)$$

This equation can be rewritten as

$$n_0^2 = 1 + \frac{hc}{\pi^2} \int_0^\infty \frac{n(E)\alpha(E)}{E^2} dE \quad (7)$$

using the well known equations  $\epsilon_2 = 2nk$ ,  $a = 4\pi k/\lambda$ , and  $E = hc/\lambda$ , where  $k$ ,  $h$ ,  $\lambda$ , and  $c$  are the extinction coefficient, Planck's constant, and the wavelength and speed of light in the film, respectively. From Figs. 5 and 7 we can readily see that increasing proportions of oxygen in the gas feed shift the  $n(E)$  curves towards lower values of  $n$  and the absorption edge of the  $a(E)$  curves towards higher energies. Thus an increase in the optical gap—which is equivalent to an increase in the oxygen content of the films—produces a negative contribution to  $n_0$  due to the decrease in the integral of Eq. (7).

#### IV. CONCLUSIONS

Amorphous oxygen-containing hydrogenated carbon films were deposited from rf discharges of mixtures of  $C_2H_2$ ,  $O_2$ ,

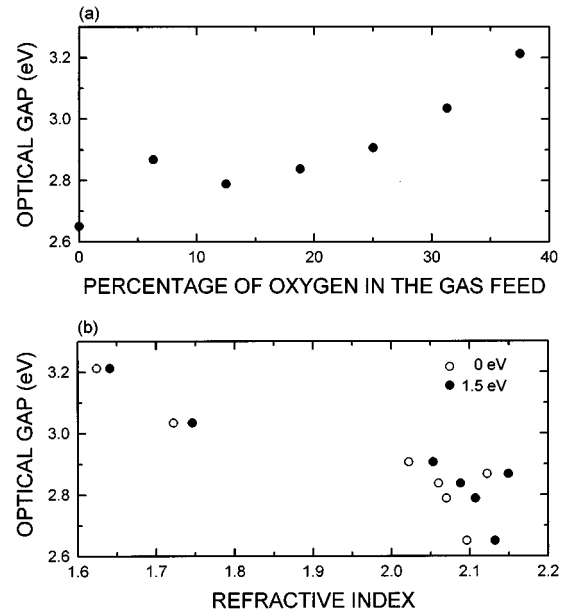


Fig. 8. Dependence of the optical gap  $E_{04}$  on the percentage of  $O_2$  in the gas feed (a) and on the refractive index (b).

and Ar at deposition rates in the range 50–30 nm/min. As confirmed by IR spectroscopy and XPS, the degree of oxygen incorporation into the films is controllable by selection of the proportion of oxygen in the feed. An oxygen to carbon atomic ratio as high as 0.40 was found for the film deposited with the highest percentage of  $O_2$  in the gas feed (37.5%). Since hydrocarbon structures were present in all the films studied, we conclude that polycarbonatelike films of high oxygen content can be formed from  $C_2H_2$ – $O_2$ –Ar discharges.

The oxygen content also influences some of the film optical parameters. As  $X_{ox}$  varies from 0% to 37.5%, a relatively large decrease in the refractive index (2.13–1.64) and an increase in the optical gap (2.62–3.21 eV) were measured. The dependence of the optical gap on the refractive index was also investigated. The results are similar to those obtained in other amorphous materials ( $a$ -Si:H and  $a$ -Si:H:N) and were interpreted in terms of a theoretical relationship linking the static refractive index to the imaginary part of the dielectric function.

#### ACKNOWLEDGMENTS

The authors thank the Conselho Nacional de Desenvolvimento Científico e Tecnológico (CNPq) of Brazil for financial support. P. R. Pedroso, A. C. Costa, and R. C. G. Vinhas provided excellent technical assistance with the IR, UVS, and XPS analyses, respectively.

<sup>1</sup>H. Yasuda, *Plasma Polymerization* (Academic, Orlando, 1985).

<sup>2</sup>J. W. Zou, K. Schmidt, K. Reichelt, and B. Dischler, *J. Appl. Phys.* **67**, 487 (1990).

<sup>3</sup>H. Tsai and D. B. Bogy, *J. Vac. Sci. Technol. A* **5**, 3287 (1987).

<sup>4</sup>H.-X. Han and B. J. Feldman, *Solid State Commun.* **65**, 921 (1988).

- <sup>5</sup>M. Ricci, M. Trinqucoste, F. Auguste, R. Canet, P. Delhaes, C. Guimon, and G. Pfister-Guillouzo, *J. Mater. Res.* **8**, 480 (1993).
- <sup>6</sup>S. F. Durrant, N. Marçal, S. G. Castro, R. C. G. Vinhas, M. A. Bica de Moraes, and J. H. Nicola, *Thin Solid Films* **259**, 139 (1995).
- <sup>7</sup>H. Z. Wang, M. W. Rembold, and J. Q. Wang, *J. Appl. Polym. Sci.* **49**, 701 (1993).
- <sup>8</sup>S. F. Durrant, R. P. Mota, and M. A. Bica de Moraes, *J. Appl. Phys.* **71**, 448 (1992).
- <sup>9</sup>S. F. Durrant, R. P. Mota, and M. A. Bica de Moraes, *Thin Solid Films* **220**, 295 (1992).
- <sup>10</sup>C. Rau and W. Kulisch, *Thin Solid Films* **249**, 28 (1994).
- <sup>11</sup>H. Yasuda, C. Marsh, M. O. Bumgarner, and N. Morosoff, *J. Appl. Polym. Sci.* **19**, 2845 (1975).
- <sup>12</sup>F. D. Egitto, V. Vukanovic, and G. N. Taylor, in *Plasma Deposition, Treatment and Etching of Polymers*, edited by R. d'Agostino (Academic, San Diego, 1990), Chap. 5.
- <sup>13</sup>G. W. Prohaska and C. G. Nickoson, *J. Polym. Sci. Polym. Chem. Ed.* **27**, 2633 (1989).
- <sup>14</sup>S. F. Durrant and M. A. Bica de Moraes, *J. Vac. Sci. Technol. A*, 2513 (1995).
- <sup>15</sup>J. H. Scofield, *J. Electron. Spec. Relat. Phenom.* **8**, 129 (1976).
- <sup>16</sup>Z. Knittl, *Optics of Thin Films* (Wiley, New York, 1976).
- <sup>17</sup>M. Born and E. Wolf, *Principles of Optics* (Pergamon, New York, 1975).
- <sup>18</sup>J. I. Cisneros, G. B. Rego, M. Tomiyama, S. Bilac, J. M. Gonçalves, A. E. Rodriguez, and Z. P. Arguello, *Thin Solid Films* **100**, 155 (1983).
- <sup>19</sup>N. Morosoff, B. Crist, M. Bumgarner, T. Hsu, and H. Yasuda, *J. Macromol. Sci. Chem. A* **10**, 451 (1976).
- <sup>20</sup>H. Yasuda and T. S. Hsu, *J. Polym. Sci. Polym. Chem. Ed.* **15**, 81 (1977).
- <sup>21</sup>H. Yasuda and T. S. Hsu, *J. Polym. Sci. Polym. Chem. Ed.* **15**, 2411 (1977).
- <sup>22</sup>H. Yasuda and H. C. Marsh, *J. Appl. Polym. Sci.* **19**, 2981 (1975).
- <sup>23</sup>D. T. Clark, B. J. Cromarty, and A. Dilks, *J. Polym. Sci. Polym. Chem. Ed.* **16**, 3173 (1978).
- <sup>24</sup>D. T. Clark and A. Harrison, *J. Polym. Sci. Polym. Chem. Ed.* **19**, 1945 (1981).
- <sup>25</sup>S. H. Wemple and M. DiDomenico, Jr., *Phys. Rev. B* **3**, 1338 (1971).
- <sup>26</sup>G. D. Cody, in *Semiconductors and Semimetals*, edited by R. K. Willardson and A. C. Beer (Academic, Orlando, 1984), Vol. 21B, Chap. 2.
- <sup>27</sup>A. R. Zanatta and I. Chambouleyron, *Phys. Rev. B* **48**, 4560 (1993).
- <sup>28</sup>E. C. Freeman and W. Paul, *Phys. Rev. B* **20**, 716 (1979).
- <sup>29</sup>J. Tauc, in *Optical Properties of Solids*, edited by F. Abeles (North-Holland, Amsterdam, 1972), Chap. 5.
- <sup>30</sup>M. M. Guraya, H. Ascolani, G. Zampieri, J. I. Cisneros, J. H. Dias da Silva, and M. P. Cantão, *Phys. Rev. B* **42**, 5677 (1990).
- <sup>31</sup>J. H. Dias da Silva, J. I. Cisneros, and M. P. Cantão, in *Current Topics in Semiconductors*, edited by O. Hipólito, A. Fazzio, and G. E. Marques (World Scientific, Singapore, 1988), p. 192.
- <sup>32</sup>J. M. Berger, C. Ance, F. de Chelle, J. P. Ferraton, A. Donnadieu, J. I. Cisneros, and J. H. Dias da Silva, *J. Non-Cryst. Solids* **94**, 353 (1987).